J. Fluid Mech. (1991), *vol.* 226, *pp.* 149–174
Printed in Great Britain

The double layer–capillary stability of an annular electrolyte film surrounding a dielectric-fluid core in a tube

By E. GEORGIOU, D. T. PAPAGEORGIOU, C. MALDARELLI AND D. S. RUMSCHITZKI†

The Levich Institute and Department of Chemical Engineering, City College of CUNY, 140th Street at Convent Avenue, New York, NY 10031, USA

(Received 19 February 1990 and in revised form 3 October 1990)

In this paper we examine the linear stability of an annular film surrounding a dielectric-fluid core in a tube in the presence of double layers of charges at the film core and at the film–tube interfaces, when the fluid–fluid interface is of low tension. In the absence of electrostatic forces, the surface tension force arising from the circumferential curvature destabilizes, and that from the axial curvature stabilizes the system. The competition is such that waves larger than the unperturbed interface circumference are unstable and those shorter are stable. For charged layers in the film, two cases are examined: (i) double-layer repulsion where the volume charge density is everywhere of the same sign and (ii) double-layer attraction where the diffusive layers next to the film interfaces are of opposite signs. In the first case, double-layer repulsion and surface tension lowering stabilize the destabilizing action of the circumferential component of the surface tension force, and a window of stability can exist. In the case of double layers of opposite signs, double-layer attraction destabilizes the system, and growth rates larger than those caused by pure capillarity can arise. Finally, for the case of a core bounded by an infinite electrolyte, surface tension lowering stabilizes the destabilizing action of the circumferential component of the surface tension force and destabilizes the longitudinal one, although the magnitudes of these effects may differ. As a result the thread can become unstable to waves shorter than the interface circumference.

1. Introduction

The goal of this study is to examine the influence of double layers of charge and capillarity on the linear interfacial stability of the static arrangement of an annular electrolyte film surrounding a dielectric core fluid in a tube, where the fluid–fluid interface is of low tension. The core–annular geometry is an excellent idealization of the flow geometries of many technologically important processes: for example lubricated pipelines (cf. Preziosi, Chen & Joseph 1989), concurrent flows in packed beds (cf. Saez, Larbeniell & Lerec 1986), coating processes and liquid–liquid displacements in the presence of a wall wetting layer, e.g. in porous media as in tertiary oil recovery. The effects discussed below are probably most relevant for the latter case. We concentrate on the static arrangement in order to isolate the effects and coupling of capillarity and double layers of charge. Flow introduces additional shear effects which can be stabilizing (Joseph, Renardy & Renardy 1984; Presiozi *et al.* 1989; Hu & Joseph 1989; Papageorgiou, Maldarelli & Rumschitzki 1990) or

† To whom correspondence should be addressed.

destabilizing (Yih 1967; Hickox 1971). A complete treatment of the stability of the core–annular geometry will include all of these effects although the insight gained from the static case is essential (as it is in the study of pure capillarity; see references below).

Capillarity governs the interfacial stability in the absence of electrostatic forces. The problem of the stability of an inviscid cylindrical thread was first studied by Plateau and then by Rayleigh (1879, 1892) neglecting the effect of a surrounding fluid. Tomotika (1935) extended these studies to include the effects of thread viscosity and an infinite outer viscous fluid, and Goren (1962) studied an annular film (with a gas interface) located on the outside or the inside surface of a tube. All of these studies indicate that for axisymmetric disturbances of the fluid interface, the circumferential component of the interfacial tension force has a destabilizing effect (large waves growing the fastest) and the axial component has a stabilizing effect (short waves damped the most). The competition is such that waves larger than the interface circumference are unstable and those smaller are stable.

When double layers of charge are present at the interface, the stability picture changes. Felderhof (1968) first studied the influence of double layers of charge within the context of the stability of thin inviscid planar electrolyte films that were symmetric about their midplane. Felderhof identified two modes of vibration of such films, a squeezing mode in which the film thickness changes and a stretching mode in which the thickness is constant. For the stretching mode Felderhof found that for long waves the double layers of charge effectively reduce the interfacial tension, thereby destabilizing the system. The reason for this reduction in the interfacial tension is that the negative electrostatic double-layer energy lowers the overall interfacial energy. For the squeezing mode, movement of the opposing interfaces towards each other brings charges of equal sign together, and Felderhof found that for long waves this double-layer repulsion strongly stabilizes the system. Various studies extended Felderhof's results to include viscous lamella. They demonstrated that, as long as the base state is one of zero flow, viscosity affects the growth rates but not the criteria for stability (for reviews see Gallez & Coakly 1986; Jain & Maldarelli 1988). Finally, Miller & Scriven (1970*a*, *b*) studied the case of single double layers of charge extending from a planar interface, and outward from a spherical interface. They found results similar to those for the stretching mode of Felderhof: for long waves, the presence of the double layer effectively lowers the surface tension and destabilizes the system. Miller & Scriven also showed that at shorter waves, the stabilizing effect of surface tension dominates while the destabilizing action of the double layers disappears.

The stability of a cylindrical interface surrounded by an electrolyte film presents several interacting effects because there are two curvatures, one stabilizing and one destabilizing, and the double layers of charge will affect each differently. The aim of this study is to establish the precise roles surface tension lowering and double-layer repulsion play in determining the cylindrical interface stability. We shall consider only axisymmetric disturbances.

This study is divided into three major sections. Section 2 formulates the linear stability problem, and derives the dispersion equation. Section 3 presents and discusses neutral curves and growth rate curves, and the study ends with a summary and some conclusions in §4.

2. Formulation of linear stability theory

2.1. *Governing equations and boundary conditions*

Two immiscible, Newtonian, incompressible fluids of equal density are resting in a core–annular arrangement in a pipe of inner radius R_2. The interface is given by $r = R_1$. A dielectric fluid of viscosity μ_1 and density ρ occupies the core region $0 \leqslant r \leqslant R_1$. A second fluid which is a univalent electrolyte with viscosity μ_2 and density ρ occupies the film region $R_1 \leqslant r \leqslant R_2$. The film electrolyte is drawn from a neutral reservoir. Axisymmetric disturbances of the interface are defined by $r(z,t) = f(z,t)$ (see figure 1).

The equations of motion and continuity in the presence of electrostatic forces and with gravity neglected are

$$\rho \frac{\mathrm{d}\boldsymbol{v}_i}{\mathrm{d}t} = -\boldsymbol{\nabla}\cdot(\boldsymbol{P}_i - \boldsymbol{T}_i) + \mu_i \nabla^2 \boldsymbol{v}_i, \tag{2.1}$$

and

$$\boldsymbol{\nabla}\cdot\boldsymbol{v}_i = 0, \tag{2.2}$$

where $i = 1$ denotes the core fluid and $i = 2$ denotes the film fluid, $\mathrm{d}/\mathrm{d}t$ is a convective derivative, $\boldsymbol{P}$ is the isotropic pressure tensor and $\boldsymbol{T}$ is the Maxwell stress tensor from electrostatics ($\boldsymbol{T}_1 = \boldsymbol{0}$). The components of $\boldsymbol{P}$ are

$$P_{ij} = p\delta_{ij}, \tag{2.3}$$

where p is the scalar pressure. The components of $\boldsymbol{T}$ are

$$T_{ij} = \frac{\epsilon_e}{4\pi} E_i E_j - \frac{(\epsilon_e - \hat{\eta})}{8\pi} E_k E_k \delta_{ij}, \tag{2.4}$$

where ϵ_e is the dielectric constant, $\boldsymbol{E}$ the electric field, and $\hat{\eta}$ a material constant which depends on the way the force is separated into mechanical and electrical parts. Two frequently used expressions for the force density are

$$\hat{\eta} = \epsilon_e - 1 \quad \text{(Kelvin)} \quad \text{and} \quad \hat{\eta} = \rho \frac{\partial \epsilon_e}{\partial \rho} \quad \text{(Helmholtz)}. \tag{2.5}$$

It turns out that, owing to the fluids' incompressibility, our final results are independent of $\hat{\eta}$ (see §2.3).

To determine the electric field in the electrolyte film, we assume that the interfacial frequencies are slow enough so as to allow the ions to be in instantaneous thermal equilibrium for all interfacial positions. The absence of volume charge density in the core leads to a uniform potential and a zero electric field and Maxwell stress tensor there. In the film, assumed to have a uniform dielectric constant ϵ_e, the electrical potential $\hat{\Phi}$, relative to the potential λ of the reservoir from which the film is drawn, satisfies (cf. Melcher 1981) for $[|\hat{\Phi} - \lambda| \ll KT/e]$,

$$\nabla^2(\hat{\Phi} - \lambda) - \frac{8\pi e^2 n_0}{\epsilon_e KT}(\hat{\Phi} - \lambda) = 0, \tag{2.6}$$

where

$$\nabla^2 \equiv \frac{\partial^2}{\partial r^2} + \frac{1}{r}\frac{\partial}{\partial r} + \frac{\partial^2}{\partial z^2}, \tag{2.7}$$

n_0 is the number density of univalent cations and anions, e is the elementary charge, K is the Boltzmann's constant and T is the absolute temperature. Let $\Phi = \hat{\Phi} - \lambda$ be the potential defined relative to λ.

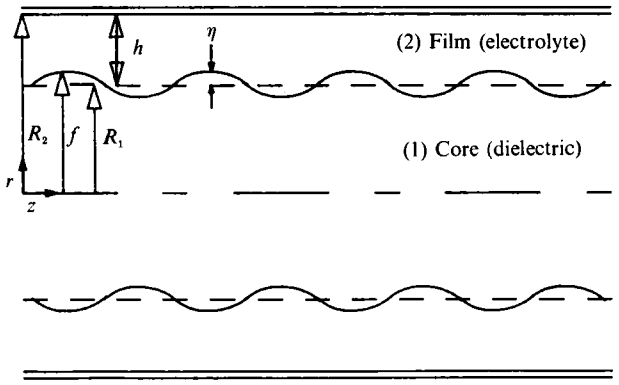

FIGURE 1. Schematic of the circular tube geometry detailing the electrolyte film and the dielectric core.

Certain boundary conditions for our system are clear: no slip at the wall $r = R_2$; the velocity field is bounded at the centreline; the velocity field is continuous at the interface $r = f(z, t)$.

Stress balances at the fluid interface must account for pressure, electrostatic, interfacial phase tension and viscous forces as well as Marangoni stresses which may occur due to gradients of the adsorbed charged species. To account for these effects in a consistent manner, we make two principal assumptions. First we assume that sorptive kinetic processes between the bulk sublayer and the surface are fast enough so that the surface and subsurface remain in equilibrium with one another despite the surface movement. The second assumption is that the interfacial thickness is much smaller than the lengthscale of the diffuse layer. According to this view, adsorption from inside the diffuse layer onto the surface is purely chemically driven. Thus we take the phase tension σ to be divorced from electrostatic forces and to depend only on the sublayer concentration $n_s^{\mp}$ of cations or anions via the usual Gibbs' adsorption relation

$$\frac{\partial \sigma}{\partial \ln n_s^{\mp}} = -KT\Gamma^{\mp}, \tag{2.8}$$

where $\Gamma^{\mp}$ is the surface concentration of cations or anions.

The tangential Marangoni stress is

$$\nabla_s \sigma = \frac{\partial \sigma}{\partial \ln n_s^+} \nabla_s \ln n_s^+ + \frac{\partial \sigma}{\partial \ln n_s^-} \nabla_s \ln n_s^-,$$

where ∇_s denotes the surface gradient operator. This stress exactly cancels the electrostatic tangential force

$$\boldsymbol{n} \cdot (\boldsymbol{T}_2 - \boldsymbol{T}_1) \cdot \boldsymbol{t} = \sigma_e \boldsymbol{E} \cdot \boldsymbol{t} = -(e\Gamma^+ - e\Gamma^-) \nabla_s \Phi_s,$$

where σ_e is the surface charge density and Φ_s the surface potential, since the bulk sublayer is in electrochemical equilibrium and therefore

$$\nabla_s (\ln (n_s^{\mp})) = \pm \frac{e}{KT} \nabla_s \Phi_s.$$

Consequently the tangential and normal stress balances at the interface are

$$\boldsymbol{n} \cdot (\bar{\boldsymbol{T}}_2 - \bar{\boldsymbol{T}}_1) \cdot \boldsymbol{t} = 0 \quad \text{at} \quad r = f(z, t), \tag{2.9}$$

and $$\boldsymbol{n}\cdot(\hat{\boldsymbol{T}}_2-\hat{\boldsymbol{T}}_1)\cdot\boldsymbol{n}=-2H\sigma \quad \text{at} \quad r=f(z,t); \tag{2.10}$$

where (2.8) in principle determines the variations in the phase tension. The kinematic condition at the interface is

$$v=\frac{\partial f}{\partial t}+w\frac{\partial f}{\partial z} \quad \text{at} \quad r=f(z,t), \tag{2.11}$$

where v and w are the r- and z-components of $\boldsymbol{v}$, respectively. In (2.9) and (2.10) $\boldsymbol{n}$ is the unit vector normal to the interface defined as positive when pointing from the core to the film and $\boldsymbol{t}$ is the tangential unit vector at the interface. In the boundary conditions $\hat{\boldsymbol{T}}_i$ is the total stress tensor

$$\hat{\boldsymbol{T}}_i=-\boldsymbol{P}_i+\bar{\boldsymbol{T}}_i+\boldsymbol{T}_i, \tag{2.12}$$

and $\bar{\boldsymbol{T}}_i$ is the fluid mechanical stress tensor

$$\bar{\boldsymbol{T}}_i=\mu_i[\nabla\boldsymbol{v}_i+(\nabla\boldsymbol{v}_i)^{\mathrm{t}}]. \tag{2.13}$$

Finally, $2H$ is the sum of the principal curvatures

$$2H=-\frac{1}{f(1+f'^2)^{\frac{1}{2}}}+\frac{f''}{(1+f'^2)^{\frac{3}{2}}}. \tag{2.14}$$

In (2.14) f' and f'' are respectively the first and second derivatives of the function $f(z, t)$ with respect to z at a given time.

To close the problem requires setting the electrical boundary conditions. In general, when sorption equilibrium is assumed, specifying the adsorption isotherm relates the surface adsorption $\Gamma^{\mp}$ to the sublayer concentration of the charged species $n_{\mathrm{s}}^{\mp}$ and thereby permits calculation of the surface's potentials. In dynamic events, we consider the limiting case of constant surface potential of both the wall and the interface:

$$\Phi(r=R_2)=\Phi_{\mathrm{w}} \quad \text{and} \quad \Phi(r=f(z,t))=\Phi_{\mathrm{I}}, \tag{2.15}$$

which requires of the isotherms that

$$\frac{\partial\Gamma^{\mp}}{\partial\Phi_{\mathrm{s}}}=\pm\frac{e}{KT}\frac{\partial\Gamma^{\mp}}{\partial\ln(n_{\mathrm{s}}^{\mp})}$$

be infinite. It is worth noting that in the case of constant surface potential, the zeroth- and first-order tangential electric fields are zero and thus the tangential electrical (and Marangoni) stresses are each individually zero. Moreover, since

$$\mathrm{d}\sigma=\left(\frac{\partial\sigma}{\partial\ln(n_{\mathrm{s}}^{+})}\frac{\partial\ln(n_{\mathrm{s}}^{+})}{\partial\Phi_{\mathrm{s}}}+\frac{\partial\sigma}{\partial\ln(n_{\mathrm{s}}^{-})}\frac{\partial\ln(n_{\mathrm{s}}^{-})}{\partial\Phi_{\mathrm{s}}}\right)\nabla_{\mathrm{s}}\Phi_{\mathrm{s}}=e(\Gamma^{+}-\Gamma^{-})\,\mathrm{d}\Phi_{\mathrm{s}},$$

constancy of Φ_{s} requires the phase tension σ in the interfacial boundary conditions to be constant as well.

We shall now make the hydrodynamic equations and boundary conditions dimensionless. We scale lengths with the inner radius R_1, velocities with $[\sigma/\mu_1]$, time with $[\mu_1 R_1/\sigma]$, pressure with $[\sigma/R_1]$, potential with $[KT/e]$ and the Maxwell stress tensor with $[(KT/eR_1)^2]$. We shall use the same symbols for dimensional and dimensionless variables.

The continuity equation is satisfied automatically by defining a stream function, Ψ, such that

$$u_i=\frac{1}{r}\frac{\partial\Psi_i}{\partial z} \quad \text{and} \quad w_i=-\frac{1}{r}\frac{\partial\Psi_i}{\partial r}. \tag{2.16}$$

Since the divergence of the Maxwell stress tensor is irrotational (cf. Felderhof 1968) for this case in which the ions are distributed in thermal equilibrium, taking the curl of (2.1) eliminates the pressure and the Maxwell stress tensor. Substituting the above expressions for u_i and w_i gives the dimensionless differential equation for Ψ_i:

$$\frac{J}{m_i}\left[\frac{\partial}{\partial t}(\mathrm{E}^2\Psi_i)-\frac{1}{r}\left(\frac{\partial\Psi_i}{\partial z}\frac{\partial}{\partial z}(\mathrm{E}^2\Psi_i)-\frac{\partial\Psi_i}{\partial z}\frac{\partial}{\partial r}(\mathrm{E}^2\Psi_i)\right)-\frac{2}{r^2}\frac{\partial\Psi_i}{\partial z}\mathrm{E}^2\Psi_i\right]=\mathrm{E}^2(\mathrm{E}^2\Psi_i), \quad (2.17)$$

where

$$\mathrm{E}^2\equiv\frac{\partial^2}{\partial r^2}-\frac{1}{r}\frac{\partial}{\partial r}+\frac{\partial^2}{\partial z^2}. \quad (2.18)$$

The dimensionless parameters

$$J\equiv\frac{\rho\sigma R_1}{\mu_1^2}, \quad m_1=1, \quad m_2=m\equiv\frac{\mu_2}{\mu_1} \quad (2.19)$$

appear in (2.17) as a result of the non-dimensionalization proposed above. J is a surface tension parameter introduced by Chandrasekhar (1968) in his study of the capillary instability of jets of a viscous liquid in air and m is the viscosity ratio of the two fluids. (The dimensionless boundary conditions are given in §2.3 in their linear form.)

2.2. *Base state*

We begin by examining the case where the interface is undisturbed. This base state velocity field is

$$u_i^0=w_i^0=0 \quad \text{for} \quad i=1,2, \quad (2.20)$$

Equation (2.6) in dimensionless form is

$$\nabla^2\Phi-\kappa^2\Phi=0, \quad (2.21)$$

where

$$\kappa^2\equiv\frac{8\pi}{\epsilon_e}\frac{e^2}{KT}n_0R_1^2 \quad (2.22)$$

defines the non-dimensional inverse Debye length. Its base state potential solution is

$$\Phi^0(r)=a_1I_0(\kappa r)+a_2K_0(\kappa r), \quad (2.23)$$

where $I_0(x)$ and $K_0(x)$ are modified Bessel functions of order zero, and a_1 and a_2 are constants to be determined by the dimensionless boundary conditions

$$\Phi^0(r=a)=\Phi_\mathrm{w}, \quad \Phi^0(r=1)=\Phi_\mathrm{I}, \quad (2.24)$$

where

$$a\equiv\frac{R_2}{R_1}. \quad (2.25)$$

We apply the two boundary conditions to get the two constants a_1 and a_2:

$$a_1=\Phi_\mathrm{I}\frac{K_0(\kappa a)-(1-\Delta\Phi/\Phi_\mathrm{I})K_0(\kappa)}{I_0(\kappa)K_0(\kappa a)-I_0(\kappa a)K_0(\kappa)}, \quad (2.26)$$

$$a_2=-\Phi_\mathrm{I}\frac{I_0(\kappa a)-(1-\Delta\Phi/\Phi_\mathrm{I})I_0(\kappa)}{I_0(\kappa)K_0(\kappa a)-I_0(\kappa a)K_0(\kappa)}, \quad (2.27)$$

where

$$\Delta\Phi=\Phi_\mathrm{I}-\Phi_\mathrm{w}. \quad (2.28)$$

2.3. *Linear stability*

We now introduce a small disturbance to the interface

$$r(z,t) = 1+\eta(z,t)\,\delta+O(\delta^2), \tag{2.29}$$

and thus to the base state

$$[\Psi(\boldsymbol{r}),P(\boldsymbol{r}),\Phi(\boldsymbol{r})] = [\Psi^1(\boldsymbol{r})\,\delta,P^0+P^1(\boldsymbol{r})\,\delta,\Phi^0(\boldsymbol{r})+\Phi^1(\boldsymbol{r})\,\delta]+O(\delta^2), \tag{2.30}$$

where δ is an ordering parameter. To determine the interface stability, we expand the first-order variables in normal modes:

$$[\Psi^1(\boldsymbol{r}),P^1(\boldsymbol{r}),\Phi^1(\boldsymbol{r})] = [\psi(r),p(r),\phi(r)]\exp[\mathrm{i}\alpha(z-ct)]. \tag{2.31}$$

We substitute (2.30) into (2.17) and (2.21), linearize with respect to δ and then substitute (2.31) to get

$$\mathrm{D}\left(\mathrm{D}\psi_i(r)+\frac{J\mathrm{i}\alpha c}{m_i}\psi_i(r)\right) = 0, \tag{2.32}$$

and

$$\frac{\mathrm{d}^2\phi}{\mathrm{d}r^2}+\frac{1}{r}\frac{\mathrm{d}\phi}{\mathrm{d}r} = \gamma^2\phi, \tag{2.33}$$

where

$$\mathrm{D}\equiv\frac{\mathrm{d}^2}{\mathrm{d}r^2}-\frac{1}{r}\frac{\mathrm{d}}{\mathrm{d}r}-\alpha^2, \tag{2.34}$$

and

$$\gamma^2 = \kappa^2+\alpha^2. \tag{2.35}$$

The boundary conditions in a linearized dimensionless form are

$$\psi_2 = 0 \quad\text{and}\quad \frac{\mathrm{d}\psi_2}{\mathrm{d}r} = 0 \quad\text{at}\quad r = a, \tag{2.36}$$

$$\psi_1 < \infty \quad\text{and}\quad \frac{\mathrm{d}\psi_1}{\mathrm{d}r} < \infty \quad\text{at}\quad r = 0, \tag{2.37}$$

$$\psi_1 = \psi_2 \quad\text{and}\quad \frac{\mathrm{d}\psi_1}{\mathrm{d}r} = \frac{\mathrm{d}\psi_2}{\mathrm{d}r} \quad\text{at}\quad r = 1, \tag{2.38}$$

$$m[\mathrm{D}\psi_2+2\alpha^2\psi_2]-[\mathrm{D}\psi_1+2\alpha^2\psi_1] = 0 \quad\text{at}\quad r = 1, \tag{2.39}$$

$$\frac{m}{\mathrm{i}\alpha r}\frac{\mathrm{d}}{\mathrm{d}r}[\mathrm{D}\psi_2]+2m\mathrm{i}\alpha\frac{\mathrm{d}}{\mathrm{d}r}\left[\frac{1}{r}\psi_2\right]-\frac{1}{\mathrm{i}\alpha r}\frac{\mathrm{d}}{\mathrm{d}r}[\mathrm{D}\psi_1]-2\mathrm{i}\alpha\frac{\mathrm{d}}{\mathrm{d}r}\left[\frac{1}{r}\psi_1\right]$$

$$+\frac{Q}{\Phi_1^2}\left[\frac{\mathrm{d}\Phi^0}{\mathrm{d}r}\frac{\mathrm{d}\phi}{\mathrm{d}r}-\phi\left(\frac{\mathrm{d}^2\Phi^0}{\mathrm{d}r^2}+\frac{1}{r}\frac{\mathrm{d}\Phi^0}{\mathrm{d}r}\right)-\left(\frac{\mathrm{d}\Phi^0}{\mathrm{d}r}\right)^2\eta\right] = [\alpha^2-1]\eta \quad\text{at}\quad r = 1, \tag{2.40}$$

$$\eta = -\frac{1}{r}\frac{\psi_1}{c}, \tag{2.41}$$

$$\phi = 0 \quad\text{at}\quad r = a \quad\text{and}\quad \phi+\eta\frac{\mathrm{d}\Phi^0}{\mathrm{d}r} = 0 \quad\text{at}\quad r = 1. \tag{2.42}$$

The dimensionless parameter Q appearing in (2.40) is the ratio of the electrostatic forces over the capillary forces:

$$Q = \frac{\epsilon_e}{4\pi}\frac{[\Phi_1 KT/e]^2}{\sigma R_1}. \tag{2.43}$$

Note that the term in the square brackets in (2.43) is just the dimensional form of Φ_1. Also, observe that, as in Felderhof (1968), $\hat{\eta}$ enters only the isotropic stress, which is substituted for and eliminated from the boundary conditions and the problem along with the pressure.

The solution to (2.32) is

$$\psi_i(r) = A_i rI_1(\alpha r) + B_i rK_1(\alpha r) + D_i rI_1(\beta_i r) + E_i rK_1(\beta_i r), \tag{2.44}$$

where

$$\beta_i^2 = \alpha^2 - \frac{Ji\alpha c}{m_i} \quad \text{for} \quad i = 1, 2. \tag{2.45}$$

The solution to (2.33) is

$$\phi(r) = a_3 I_0(\gamma r) + a_4 K_0(\gamma r). \tag{2.46}$$

We first apply the two electrostatic boundary conditions (2.42) to get the constants a_3 and a_4 in terms of η:

$$a_3 = \frac{K_0(\gamma a)\,\kappa[a_1 I_1(\kappa) - a_2 K_1(\kappa)]}{K_0(\gamma) I_0(\gamma a) - K_0(\gamma a) I_0(\gamma)}\eta, \tag{2.47}$$

$$a_4 = -\frac{I_0(\gamma a)\,\kappa[a_1 I_1(\kappa) - a_2 K_1(\kappa)]}{K_0(\gamma) I_0(\gamma a) - K_0(\gamma a) I_0(\gamma)}\eta. \tag{2.48}$$

From (2.46), (2.47) and (2.48) we get $\phi(r)$ in terms of η.

Substituting (2.23), (2.26), (2.27), (2.41), (2.44), (2.46), (2.47) and (2.48) into (2.36)–(2.40) we get a (6×6) system of equations of the form

$$\boldsymbol{A}\boldsymbol{x} = \boldsymbol{0}. \tag{2.49}$$

The matrix $\boldsymbol{A}$:

$$\begin{bmatrix}
0 & 0 & I_1(\alpha a) & K_1(\alpha a) & I_1(\beta_2 a) & K_1(\beta_2 a) \\
0 & 0 & \alpha I_0(\alpha a) & -\alpha K_0(\alpha a) & \beta_2 I_0(\beta_2 a) & -\beta_2 K_0(\beta_2 a) \\
I_1(\alpha) & I_1(\beta_1) & -I_1(\alpha) & -K_1(\alpha) & -I_1(\beta_2) & -K_1(\beta_2) \\
\alpha I_0(\alpha) & \beta_1 I_0(\beta_1) & -\alpha I_0(\alpha) & \alpha K_0(\alpha) & -\beta_2 I_0(\beta_2) & \beta_2 K_0(\beta_2) \\
(m-1)\,2\alpha^2 & (m-1)\,2\alpha^2 I_1(\beta_1) & 0 & 0 & \omega J I_1(\beta_2) & \omega J K_1(\beta_2) \\
\times I_1(\alpha) & -\omega J I_1(\beta_1) & & & & \\
F_1 I_1(\alpha) & F_1 I_1(\beta_1) & 2m\alpha^2 I_0(\alpha) & -2m\alpha^2 K_0(\alpha) & -F_3 I_0(\beta_2) & F_3 K_0(\beta_2) \\
-2\alpha^2 I_0(\alpha) & +F_2 I_0(\beta_1) & -2m\alpha I_1(\alpha) & -2m\alpha K_1(\alpha) & -2m\alpha I_1(\beta_2) & -2m\alpha K_1(\beta_2)
\end{bmatrix}$$

in (2.49) contains the coefficients of the constants of integration from the linearized boundary conditions. The constants appearing in $\boldsymbol{A}$ are

$$F_1 = \frac{1 - \alpha^2 + Q\mathscr{E}}{\omega}\alpha + 2\alpha, \tag{2.50}$$

$$F_2 = \left(J\frac{\omega}{\alpha} - 3\alpha\right)\beta_1, \tag{2.51}$$

$$F_3 = \left(J\frac{\omega}{\alpha} - 2m\alpha\right)\beta_2, \tag{2.52}$$

where ω is the growth rate

$$\omega = -i\alpha c, \tag{2.53}$$

and where $\mathscr{E}$ reflects the electrostatic contribution to the stability of our system in the normal stress balance

$$\mathscr{E} = \frac{\Phi_r^0}{\Phi_I^2}\left(\frac{K_0(\gamma a)I_1(\gamma)+I_0(\gamma a)K_1(\gamma)}{I_0(\gamma a)K_0(\gamma)-I_0(\gamma)K_0(\gamma a)}\gamma\Phi_r^0+\Phi_{rr}^0\right). \tag{2.54}$$

In (2.54) Φ_r^0 and Φ_{rr}^0 are the first and second derivatives of the base state electrostatic potential Φ^0 at the interface, which are

$$\Phi_r^0 = \kappa(a_1 I_1(\kappa)-a_2 K_1(\kappa)), \tag{2.55}$$

$$\Phi_{rr}^0 = \kappa[a_1(\kappa I_0(\kappa)-I_1(\kappa))+a_2(\kappa K_0(\kappa)+K_1(\kappa))]. \tag{2.56}$$

Finally $\boldsymbol{x}$ is the vector of the constants of integration

$$\boldsymbol{x} = [A_1, D_1, A_2, B_2, D_2, E_2]^t. \tag{2.57}$$

The stability of the system is determined by the implicit equation for $\omega(\alpha)$ which we can write as

$$\det(\boldsymbol{A}) = 0. \tag{2.58}$$

Below we solve (2.58) numerically to get a dispersion equation of the form

$$\omega = F\left(\alpha, a, J, m, Q, \kappa, \frac{\Delta\Phi}{\Phi_I}\right). \tag{2.59}$$

We will choose to represent neutral curves as the electrostatic parameter Q versus the wavenumber α with the other dependences in (2.59) as parameters. Since the neutral states are non-flowing, these neutral curves, unlike the growth rates, will be independent of the fluid mechanical parameters J and m.

3. Results

Using the LINPACK subroutines ZGECO and ZGEDE, we solve (2.58) numerically for the three cases that title the forthcoming subsections. In the results detailed here, the computed values of c are always purely imaginary (i.e. the calculated real parts are typically many orders of magnitude smaller than the calculated imaginary parts) and thus disturbances do not propagate. This is expected because the base state is one of zero flow. In the calculations given below, a new parameter ϵ given by,

$$\epsilon = \frac{R_2-R_1}{R_2} \quad \text{or} \quad \epsilon = 1-\frac{1}{a}, \tag{3.1}$$

enters to replace a.

3.1. *Pure capillarity* ($Q = 0$)

In this section we present the results in the absence of electrostatic effects which follow by setting Q equal to zero. The remaining parameters that determine the stability of the system are the surface-tension parameter J, the viscosity ratio m and the film thickness parameter ϵ. Figures 2(*a*)–2(*c*) are typical growth rate versus wavenumber curves which illustrate the dependence of ω_r *vs.* α on these groups. Each of these shows the universal and well-known behaviour that waves smaller than the interfacial circumferences are stable while all other are unstable and there is a fastest growing wave. These curves are new; they extend the results of Goren to include the influence of a core fluid.

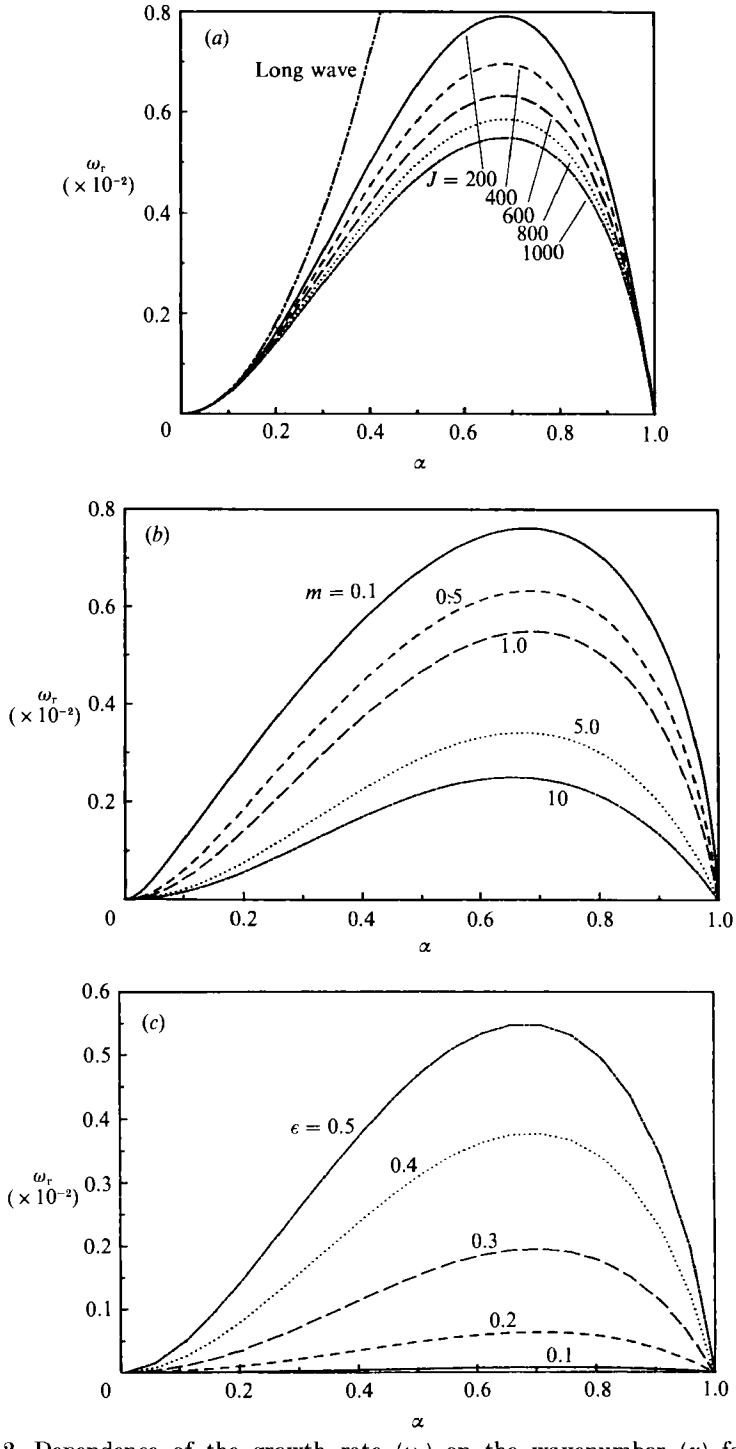

FIGURE 2. Dependence of the growth rate (ω_r) on the wavenumber (α) for capillary-driven instability: (*a*) J-dependence and the long-wave expansion, $\epsilon = 0.5$, $m = 1$, $Q = 0$; (*b*) m-dependence, $\epsilon = 0.5$, $J = 1000$, $Q = 0$; and (*c*) ϵ-dependence, $J = 1000$, $m = 1$, $Q = 0$.

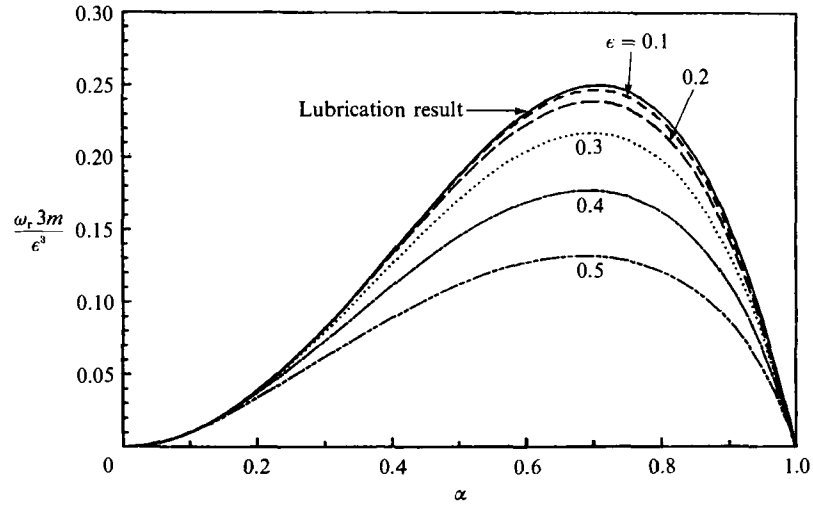

FIGURE 3. Comparison of the lubrication result (3.6) and the exact numerical solution ($\epsilon = 0.1, 0.2, 0.3, 0.4, 0.5$). $J = 1000$, $m = 1$, $Q = 0$.

As shown in figure 2(*a*), increasing J retards the growth. The simplest way to understand figure 2(*a*) is to note that since time is written in units of $[\mu_1 R_1/\sigma]$ and the wavenumber in units of $[1/R_1]$, increasing J in this figure can only be interpreted, in terms of physical variables, as increasing ρ. Since this increases the fluids' inertia, the unstable growth rates should decrease, as figure 2(*a*) demonstrates. Figure 2(*b*) shows that increasing m also has a retarding effect. This is because, with μ_1 held fixed, increasing m corresponds to increasing the film fluid's viscosity and the additional fluid resistance slows the growth. On the other hand by increasing ϵ with R_1 fixed one increases the film's thickness. This decreases the viscous resistance in the film, allowing the instability to grow faster (see figure 2*c*).

As a way of checking our numerical results we introduce the asymptotic expansion for long waves ($\alpha \to 0$) used by Yih (1967),

$$c = c^{(0)} + c^{(1)}\alpha + O(\alpha^2), \tag{3.2}$$

$$\psi = \psi^{(0)} + \psi^{(1)}\alpha + O(\alpha^2), \tag{3.3}$$

and

$$\phi = \phi^{(0)} + \phi^{(1)}\alpha + O(\alpha^2), \tag{3.4}$$

into the governing equations and solve for the leading-order term in c. The first non-vanishing term, $c^{(1)}$, in this expansion is found to be purely imaginary and is given by $c^{(1)} = c_h^{(1)}$ where

$$c_h^{(1)} = -\left[\frac{4(a^4+m-1)\log(a) + (m-4)a^4 + (8-4m)a^2 + 3m - 4}{16(ma^4+m^2-m)}\right]\mathrm{i}. \tag{3.5}$$

(We arrive at (3.5) as the result for leading order in α in two ways. In the first we substitute the above expansions (3.2) to (3.4) into the Orr–Sommerfeld equation and solve the leading-order problems sequentially. Alternatively, we begin by separating the modified Bessel functions in the exact equation (2.49) into its logarithmic and power series terms. The symbolic algebraic calculations (using MACSYMA) reveal that all terms logarithmic in α cancel identically and lead to (3.5). This results justifies the proposed expansions (3.2)–(3.4) as simple power series in α.)

The asymptotic expression (3.5) appears in figure 2(*a*) along with the exact results; the agreement for long waves is evident. Both the asymptotic and the exact results indicate that the growth rate becomes independent of J for long waves. This is because the dynamics at long waves becomes lubrication-like, and the influence of the fluids' inertia becomes negligible.

With the exact results we are in the position to assess how well lubrication theory describes the system dynamics for thin films (in the limit of $\epsilon \to 0$). In lubrication theory the radial lengthscale in the film is smaller than the axial scale and it easily follows (see Frenkel *et al.* 1987) that, for m, α and J of order one (in ϵ), the growth rate is given by

$$\omega_r = \frac{\epsilon^3}{3m}(\alpha^2 - \alpha^4). \tag{3.6}$$

Figure 3 is a comparison of the lubrication result and the exact solution. Clearly the agreement is exceptional even for ϵ as large as 0.2 for the parameters chosen. Finally, in the limit of $\epsilon \to 0$, the Yih result should coincide with the order-α^2 term in the lubrication expression; in fact, a straightforward expansion of (3.5), in powers of ϵ for $a = 1/(1-\epsilon)$, confirms that it does.

3.2 *The influence of a double layer of charge for an infinite outer region* ($Q \neq 0, \epsilon \to 1$)

In this section we include the effect of the electrostatic double layers ($Q \neq 0$) for the case of an infinite outer region ($\epsilon \to 1$). In this limit the dispersion equation depends only on the parameters J, m, κ and Q. Thus only the double layer around the interface contributes to the stability, and the sign of the interface potential does not effect the stability of the system.

The non-oscillatory neutral curves for this system derive solely from the normal stress balance and are given by

$$Q\mathscr{E} + 1 - \alpha^2 = 0, \tag{3.7}$$

where $\mathscr{E}$ is the electrostatic contribution given generally by (2.54) and specifically in the limit $\epsilon \to 1$ by

$$\mathscr{E}_\infty = \frac{\kappa^2 K_1(\kappa)}{(K_0(\kappa))^2}\left[\frac{\gamma K_1(\kappa) K_1(\gamma)}{K_0(\gamma)} - \kappa K_0(\kappa) - K_1(\kappa)\right]. \tag{3.8}$$

As noted they are independent of the hydrodynamics and are a function of the electrical parameters Q and κ only. For $Q = 0$ the capillary instability of Tomotika (1935) obtains and the system is stable only to disturbances having $\alpha \geqslant 1$.

As the dimensional interfacial radius $R_1 \to \infty$, the system becomes planar. Equation (3.7) with dimensional variables and with leading-order, large-argument expansions of the Bessel functions (e.g. Abramowitz & Stegun 1972) gives

$$-\alpha^2\sigma + \frac{\epsilon_e}{4\pi}\Phi_1^2\kappa^2(\gamma-\kappa) + \frac{\epsilon_e}{4\pi}\Phi_1^2\kappa(\gamma-\kappa)\frac{1}{R_1} + \left[\sigma + \frac{\epsilon_e}{4\pi}\Phi_1^2\left(\frac{\kappa^2 - 9\gamma\kappa + 6\gamma^2}{16\gamma}\right)\right]\frac{1}{R_1^2} + O\left(\frac{1}{R_1^3}\right) = 0. \tag{3.9}$$

As $R_1 \to \infty$ (with $\zeta = \gamma/\kappa$), it becomes

$$\alpha^2\sigma - \frac{\epsilon_e}{4\pi}\Phi_1^2\kappa^3(\zeta - 1) = 0. \tag{3.10}$$

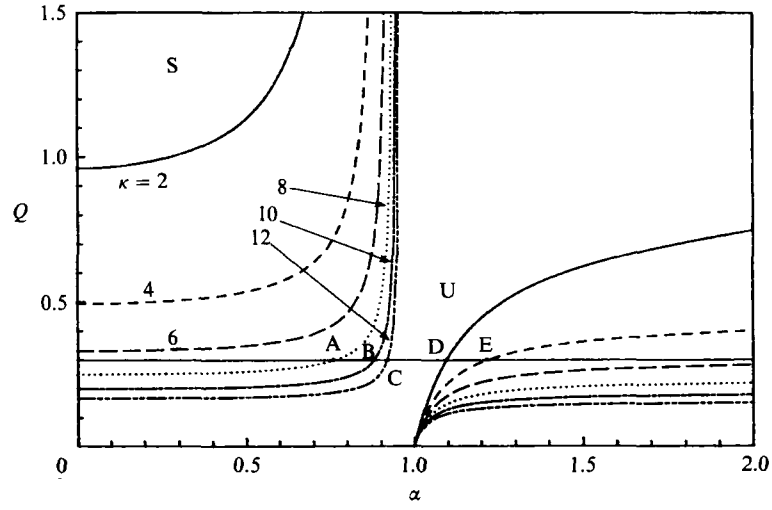

FIGURE 4. The κ-dependence of the neutral stability curves of Q against α for an infinite outer region containing a double layer.

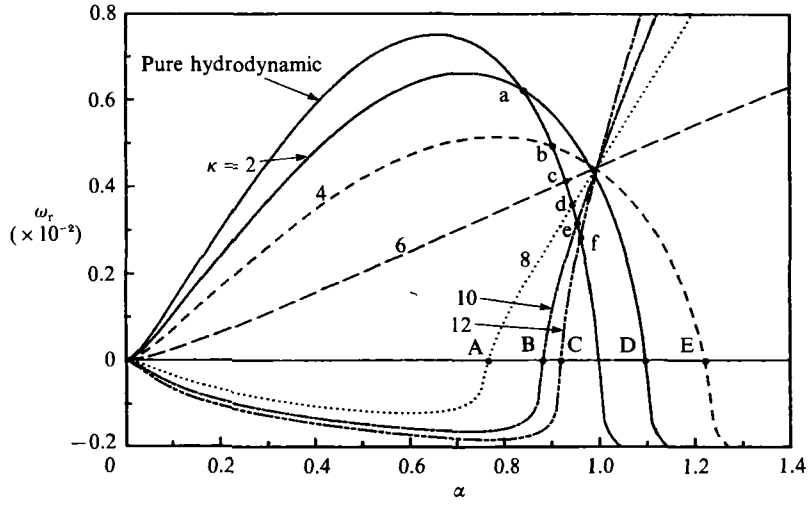

FIGURE 5. The κ-dependence of infinite-outer-region growth rate curves (ω_r *vs.* α). $Q = 0.3$, $J = 1000$, $m = 1$.

This recovers Miller & Scriven's (1970*a*, *b*)) planar, constant surface potential, marginal interfacial stability result for two fluids with equal densities.

Figure 4 shows neutral curves for different values of the inverse Debye length parameter κ. For comparison figure 5 shows growth rate curves for the same values of κ at a particular value of Q ($Q = 0.3$) and for $J = 10^3$ and $m = 1$. The crossing points of the $Q = 0.3$ line with the neutral curves of figure 4 agree perfectly with the changes of sign of the growth rate curves of figure 5. Figure 5 also includes the growth rate curve for pure hydrodynamics $Q = 0$ in which case the system is stable for $\alpha \geqslant 1$. The intersections of the pure hydrodynamic growth rate curve with the other growth rate curves (points a, b, c, d, e, and f in figure 5) are the points where the electrostatic contribution is zero ($\mathscr{E}_\infty = 0$) since even for the dynamic case, the

influence of the double layer enters only through the parameter $\mathscr{E}_\infty$. Since $\mathscr{E}_\infty$ is zero at these points, from (3.7), they coincide with the neutral curves' singular points manifest in figure 4.

To interpret the marginal curves, consider first long and moderately long waves. A short calculation shows that as $\alpha \to 0$ the electrostatic contribution $\mathscr{E}_\infty$ up to order α^2 is

$$\mathscr{E}_\infty = -b_0 + b_2 \alpha^2, \tag{3.11}$$

where b_0 and b_2 are given by

$$b_0 = -\frac{\kappa^2 K_1(\kappa)}{(K_0(\kappa))^2}\left[\frac{\kappa (K_1(\kappa))^2}{K_0(\kappa)} - \kappa K_0(\kappa) - K_1(\kappa)\right], \tag{3.12}$$

and

$$b_2 = \frac{\kappa^2 (K_1(\kappa))^2}{(K_0(\kappa))^2}\left[\frac{\kappa^2 K_0(\kappa) K_3(\kappa) - 2\kappa^2 K_1(\kappa) K_2(\kappa) + (\kappa^2 - 8) K_0(\kappa) K_1(\kappa)}{8\kappa (K_0(\kappa))^2}\right]. \tag{3.13}$$

Numerical calculation shows that, for every κ, b_0 and b_2 are both positive and b_2 is always greater than b_0 ($b_2 > b_0 > 0$).

By inserting the above expansion into the neutral stability equation (3.7) the following criterion for stability emerges for long and moderate waves:

$$\begin{aligned} (1 - Qb_0) - (1 - Qb_2)\alpha^2 < 0 \quad &\text{(stable)} \\ > 0 \quad &\text{(unstable).} \end{aligned} \tag{3.14}$$

Thus for this range of wavelengths one can interpret the electrostatic influence as a pure reduction of the surface tension for both the circumferential and the longitudinal curvature. However, the reduction in the surface tension corresponding to each of these curvatures is different, it being Qb_0 for the circumferential and Qb_2 for the longitudinal. From figure 4 and the above expansion we see that, for very long waves, only the order-α^0 terms in (3.14) are important. If Q is larger than a critical value $Q^* = 1/b_0$ the destabilizing effect of the circumferential curvature can be eliminated and the system becomes stable to such disturbances. However, at some wavenumber α^*,

$$\alpha^* = \left(\frac{1 - Qb_0}{1 - Qb_2}\right)^{\frac{1}{2}}, \tag{3.15}$$

the fact that the corresponding longitudinal tension is negative ($1 - Qb_2 < 0$ and $b_2 > b_0$) causes the system to become unstable for shorter wavelength disturbances (see figure 4, points A, B and C). Figure 5 also includes this effect; for the chosen value of Q ($Q = 0.3$) the last three growth rate curves ($\kappa = 8$, 10 and 12) start as negative (stable) and then at some wavenumber they become positive (unstable) (see figure 5, points A, B and C). For even shorter waves the system becomes stable again because the lower right branches of the neutral curves asymptote to infinity. This behaviour is given analytically by

$$\underset{\alpha \to \infty}{\mathscr{E}_\infty} = \left[\frac{\kappa K_1(\kappa)}{K_0(\kappa)}\right]^2 \alpha + O(\alpha^0); \quad \underset{\alpha \to \infty}{Q} = \left[\frac{K_0(\kappa)}{\kappa K_1(\kappa)}\right]^2 \alpha + O(\alpha^0). \tag{3.16}$$

A physical interpretation is in order. For very short waves $\mathscr{E}$ is positive (destabilizing) and linear in α. The asymptote of the lower branch, described by (3.16), becomes a balance of the order-α^2 stabilization of the longitudinal curvature and this order-α destabilization of $\mathscr{E}$. Thus at high α the electrostatic destabilization has been reduced from order-α^2 (cf. (3.14)) to order-α. As in Miller & Scriven's case, wave–wave

interactions of double layers at very short wavelengths account for this suppression of electrical destabilization, allowing surface tension's stabilization to dominate in this regime.

If, on the other hand, Q is less than $1/b_0$, the stabilizing electrostatic effect does not overcome the unstable nature of the circumferential curvature and the system is unstable for the longest waves (i.e. for $(1-Qb_0) > 0$). For this case there are two possibilities: (i) $Qb_2 < 1$ or (ii) $Qb_2 > 1$. If $Qb_2 < 1$, then the longitudinal surface tension $(1-Qb_2)$ is positive and stabilizes the system at a value of α given by (3.15) (see figures 4 and 5, points D and E), or, in fact, the purely hydrodynamic point $(\alpha, Q) = (1, 0)$.) Since $b_2 > b_0$, $\alpha^* > 1$, which accounts for the receding of the critical wavenumber to shorter waves relative to the pure hydrodynamics. Moreover, the electrical effect is stabilizing to the left of $\bar{\alpha}$: $\mathscr{E}_\infty(\bar{\alpha}) = 0$, and destabilizing to its right. Thus since $\bar{\alpha} < 1$, the points $(\alpha, Q) = (0, 1/b_0)$ and $(1, 0)$ have qualitatively different behaviour with increasing Q and therefore cannot lie on the same branch of the neutral curve.

If $Qb_2 > 1$, then the longitudinal surface tension is negative and also destabilizes the system. In this range of Q $(1/b_0 > Q > 1/b_2)$ the system never becomes stable in the quadratic range ((3.15) has no real roots), but it does become stable at higher α because of unfavourable wave–wave interactions described by (3.16) and discussed above. This accounts for the sudden flattening of the right branches of the neutral curves in figure 4 and explains why the $(Q = 0.3)$ line does not intersect the $(\kappa = 6)$ neutral curve in the quadratic range.

From figure 4 it appears that the larger the Debye length (the smaller the κ) the larger the Q has to be in order for the electrostatic contribution to stabilize for long waves or to destabilize for short waves. This can be explained as follows: at constant potential the Debye length is a measure of the length over which the electrostatic potential changes from its interfacial value due to absorbed ions to its reference value far from the interface. Thus a larger Debye length defines a weaker gradient of the base state potential Φ^0, i.e. a weaker electric field. Clearly, then, a larger Q is needed to achieve the critical electrostatic effect.

It is worth noting that these results apply equally well to the problem of a jet of uniform velocity in a vacuum or a gas. By a simple coordinate transformation, one can see that the growth rate in the case of a jet differs from our results solely by the addition of an imaginary part equal to the jet's velocity. Jet problems in the presence of axial electric fields have been the subject of previous investigators (Saville 1970, 1971; Melcher & Taylor 1969).

3.3 *The influence of a double layer of charge for a finite outer region* $(Q \neq 0, R_2 < \infty)$

In this section we present the results for the most general case, where the outer region is finite and the electrostatic effects are present. These results reduce to those of §3.1 when $Q = 0$ and to the results of §3.2 when $\epsilon \to 1$. This dispersion equation of this section depends on all the parameters ϵ, J, m, κ, Q and $\Delta\Phi/\Phi_I$.

The non-oscillatory neutral curves again obtain from (3.7) with $\mathscr{E}$ given by the general expression (2.54). As before, the neutral curves are independent of the hydrodynamics but are now functions of the film parameter ϵ and the electrical parameter $\Delta\Phi/\Phi_I$ as well as of Q and κ. Two cases have qualitatively different neutral curves and thus merit independent discussions. The first case is when the base state volume charge density is everywhere of the same sign. Interfacial perturbations cause unfavourable like-charge interactions between the interfacial and wall double layers in the regions where the perturbation has thinned the film.

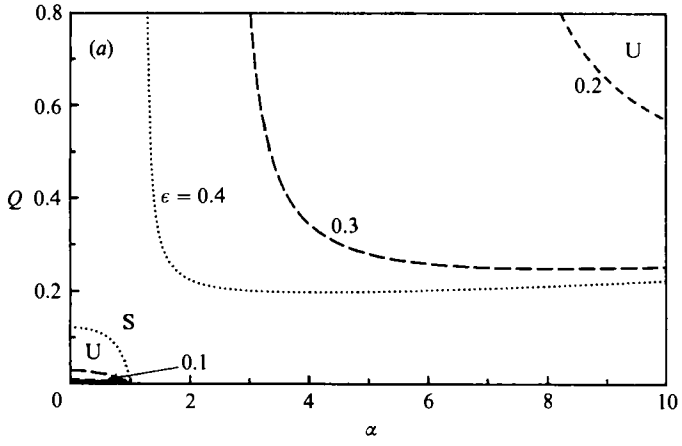

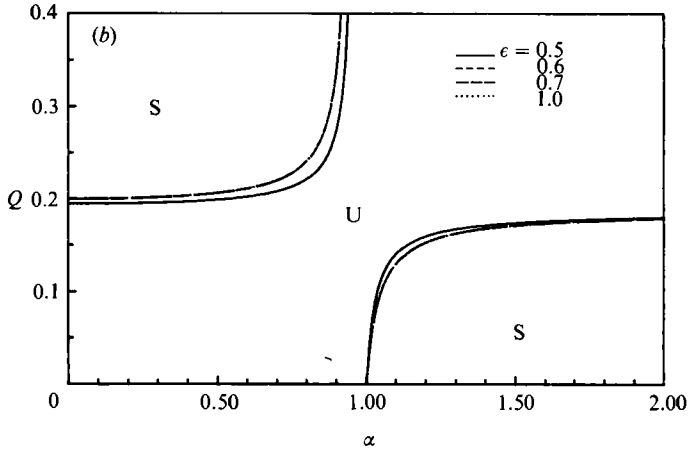

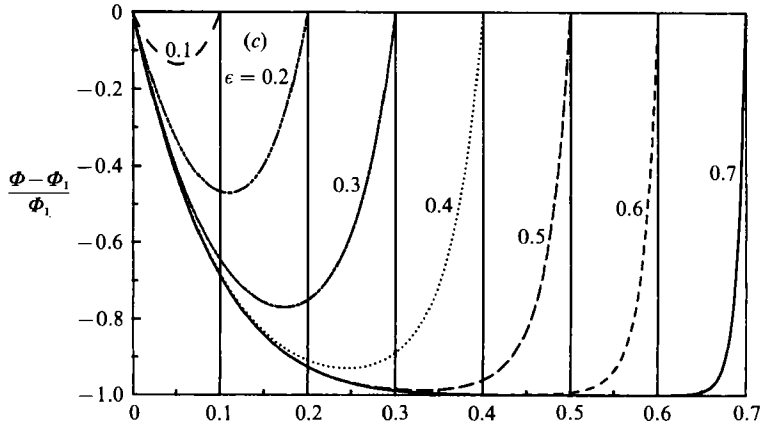

FIGURE 6(*a–c*). For caption see facing page.

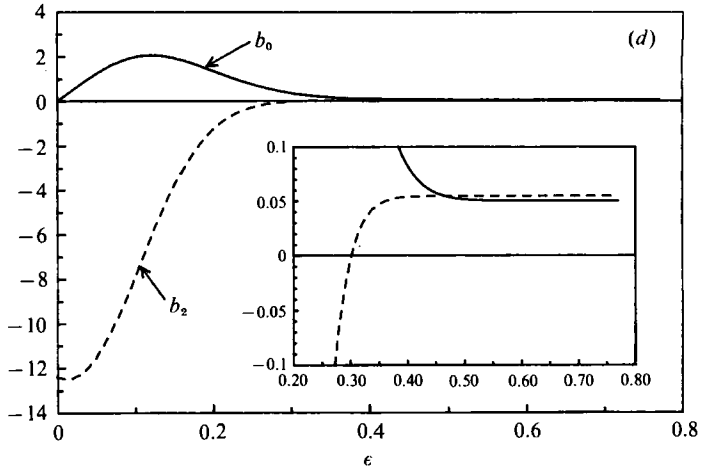

FIGURE 6. The ϵ-dependence of the stability of an electrolyte film for $\Delta\Phi/\Phi_1 = 0$, $\kappa = 10$. (*a*) Neutral curves of type A for strong double-layer repulsion ($\epsilon = 0.1, 0.2, 0.3, 0.4$). (*b*) Neutral curves of type B for weak double-layer repulsion ($\epsilon = 0.6, 0.7, 1.0$). (*c*) Base state electrostatic potential profiles for different ϵ. (*d*) Dependence of leading-order terms in the expansion of $\mathscr{E}$ (3.11) as a function of ϵ.

These interactions stabilize the system and motivate the name double-layer repulsion. In the second case, the diffuse layer adjoining the fluid interface is opposite in sign to that next to the wall. Here film thinning leads to favourable interactions between these opposite charges and this tends to destabilize the system. This case is referred to as double-layer attraction.

3.1.1. *Double-layer repulsion*

The non-dimensional base state volume charge density ρ_e^0, non-dimensionalized with en_0, is given by

$$\rho_e^0(r) = -2\Phi^0(r). \tag{3.17}$$

It is clear from (3.17) that ρ_e^0 is everywhere of the same sign as long as $\Phi^0(r)$ has that property. This can be realized when $\Delta\Phi/\Phi_1 \leqslant 1$. For discussion purposes, in this subsection we shall chose the simplest case of $\Delta\Phi/\Phi_1 = 0$. Two types of neutral curves (A and B) exist. Type B neutral curves are similar to those from the previous section where a singularity appears at some $\alpha < 1$. Type A neutral curves are new; a singularity appears at some $\alpha > 1$. These curves appear in figures 6(*a*) and 6(*b*) which vary ϵ at fixed κ. Figure 6(*c*) shows corresponding potential profiles for the values of ϵ, κ and $\Delta\Phi/\Phi_1$ chosen.

As in the previous section, expanding the parameter $\mathscr{E}$ in powers of α up to order α^2 greatly aids in the explanation of the resulting curves; thus $\mathscr{E} = -b_0 + b_2\alpha^2$, where

$$b_0 = -\frac{\Phi_r^0}{\Phi_1^2}\left(\frac{K_0(\kappa a)I_1(\kappa) + I_0(\kappa a)K_1(\kappa)}{I_0(\kappa a)K_0(\kappa) - I_0(\kappa)K_0(\kappa a)}\kappa\Phi_r^0 + \Phi_{rr}^0\right), \tag{3.18}$$

and b_2 is detailed in the Appendix. Again from (3.7), the system is stable to long- and modcrate-wavelength disturbances when $(1 - Qb_0) - (1 - Qb_2)\alpha^2$ is less than zero, and unstable to such disturbances when this parameter is greater than zero. Consider first the neutral curves in figures 6(*a*) and 6(*b*) which describe the influence of changing the film thickness with the Debye length (κ) held fixed. When ϵ is large ($\epsilon \geqslant 0.5$) the film is thick enough for the Debyc length chosen ($\kappa = 10$) so that the diffuse double

layers adjoining the interface and wall effectively do not interact and a region of nearly zero volume charge density exists (cf. figure 6*c*). Only the double layer next to the interface affects the stability, and marginal curves like those of the infinite outer region case obtain. As in that case b_0 and b_2 are both positive and b_2 is greater than b_0 ($b_2 > b_0 > 0$). For $Q > 1/b_0$ the system is stable for small α, then becomes unstable (at α^* as given by (3.15)) and finally becomes stable due to the asymptotic behaviour of $\mathscr{E}$ as $\alpha \to \infty$ given by

$$\underset{\alpha\to\infty}{\mathscr{E}} = \left[\frac{\Phi_r^0}{\Phi_1}\right]^2 \alpha + O(\alpha^0). \tag{3.19}$$

For $Q < 1/b_0$ long waves are unstable and then eventually stabilize at α^* as given by (3.15) if $Qb_2 < 1$ and outside the quadratic range if $Qb_2 > 1$. As can be seen in figure 6(*b*) the neutral curves for $\epsilon = 0.6$ and above quickly merge in to the infinite case curve ($\epsilon \to 1$).

When ϵ is less than 0.5 the region of zero volume change density in the film disappears, and the double layers interact (cf. figure 6*c*). This interaction stabilizes the system increasing b_0 (for $\epsilon > 0.1$) and decreasing b_2 as ϵ decreases (cf. figure 6*d*). (As $\epsilon \to 0$, b_0 and b_2 go to zero because the base state potential profiles become flat.) As b_2 becomes less than b_0, the two-branch neutral stability structure transforms from that of figure 6(*b*) to that of figure 6(*a*). For the longest waves, the stability is qualitatively unchanged in figure 6(*a*) from figure 6(*b*) since only b_0 is relevant there. For $Q > 1/b_0$, the system is stable while for $Q < 1/b_0$ it is unstable. However, since $b_2 < b_0$, $\alpha^* < 1$ in (3.15) for $Q < 1/b_0$ and the critical wavenumber shifts to longer waves. Since the singularity in the neutral curve, i.e. the $\bar{\alpha}$ for which $\mathscr{E}(\bar{\alpha})$ changes sign, is now to the right of 1, the electrical effect is stabilizing for all $\alpha < 1$ with the magnitude of this stabilization increasing with Q. Thus one branch of the neutral curve can connect the points $(\alpha, Q) = (0, 1/b_0)$ and $(1, 0)$; the axial curvature stabilizes the system at small $\alpha\,(< 1)$ and a small unstable lobe replaces the large unstable region between the branches of figure 6(*b*). For $Q > 1/b_0$, long waves are stable. Importantly, a window of stability for all α exists from the value $(1/b_0)$ to the minimum of the upper branch, which cannot be in the quadratic range. Note that the window widens as ϵ decreases and double-layer repulsion becomes more dominant.

Lastly, for Q above the minimum the system is destabilized at smaller waves. This may be attributed to the change in sign of the coefficient of the axial curvature $1 - Qb_2 < 0$ as well when $b_2 > 0$ ($\epsilon = 0.4$); this part of the upper branch is given by (3.15) which is in the quadratic range. For smaller ϵ however, b_2 is negative (cf. figure 6*d*) and the axial curvature is stabilizing for all Q. Thus for all these cases the transition to the unstable region for moderate α must be attributed solely to higher-order terms in α in the expansion of $\mathscr{E}$. Here too unfavourable wave–wave interactions restabilize the system to the shortest-wavelengths disturbances, reducing the dependence of $\mathscr{E}$ on α to order-α from order-α^2 (cf. (3.19)). For this part of the upper branch the marginal point is determined as the competition between the order-α destabilization caused by $\mathscr{E}$ and the order-α^2 stabilization caused by the axial curvature.

The dependence of the neutral curves on κ at fixed ϵ for the potential distributions (not shown) is similar to that of figures 6(*a*) and 6(*b*): as κ decreases at fixed ϵ, the double layers interact more and a transition occurs from the marginal curve structure of the infinite case (type B as in figure 6*b*) to that of type A (as in figure 6*a*). In the next subsection on double-layer attraction we discuss further the relationship between small ϵ and large κ.

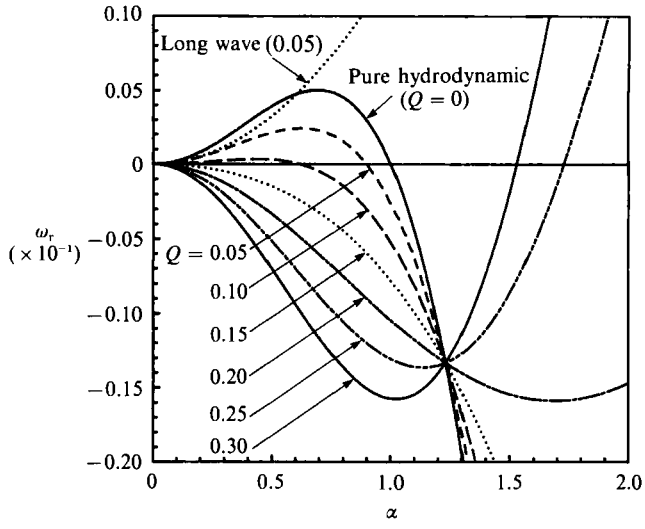

FIGURE 7. Growth rate curves as a function of Q for double-layer repulsion. $\epsilon = 0.4$, $J = 10$, $m = 1$, $\kappa = 10$, $\Delta\Phi/\Phi_1 = 0$.

The influence of double-layer repulsion on the growth rate appears in figure 7 as ω_r as a function of Q with $\Delta\Phi/\Phi_1 = 0$ and with κ, ϵ, J, and m fixed. Also plotted on the figure (for $Q = 0.05$) is the long-wave (Yih 1967) expansion for ω_r obtained from (3.2)–(3.4). Again $c^{(0)} = 0$, and $c^{(1)}$ is purely imaginary and given by

$$c^{(1)} = c_h^{(1)}(1 - Qb_0), \tag{3.20}$$

where $c_h^{(1)}$ is the same as in (3.5). The Yih approximation, which is J-independent, and the numerically exact solution converge as $\alpha \to 0$. Figure 7 clearly shows three different behaviours. When $Q < 1/b_0$, the system is unstable for a band of long waves. These are located inside the unstable lobe of figure 6*a* ($\epsilon = 0.4$). For these values of Q, it is clear that double-layer repulsion has retarded the growth rate relative to the growth rate exclusively due to capillarity (cf. the pure hydrodynamic curve). For $1/b_2 > Q > 1/b_0$ the window of stability exists and this is shown by the always-stable ($\omega_r < 0$, $Q = 0.15$) growth rate curve. Finally, for $Q > 1/b_2$, the upper branch of the type A neutral curves becomes important and positive growth rates occur at wavenumbers greater than 1 ($\alpha > 1$), although they must again stabilize for sufficiently large α ($\omega_r \to -\infty$ as $\alpha \to \infty$). Importantly, the growth rates derived from the upper-branch unstable band are much larger than the pure hydrodynamic rate ($Q = 0$). Again the intersections of the pure hydrodynamic curve with the ($Q \neq 0$) curves defines the value of $\alpha(\bar{\alpha})$ at which the electrostatic contribution is zero ($\mathscr{E}(\bar{\alpha}) = 0$). Since $\mathscr{E}$ is only a function of ϵ, κ and $\Delta\Phi/\Phi_1$ and because these parameters are fixed in figure 7, all the curves intersect at the same value of α. This value of α defines the singularity that separates the upper and lower branches of the marginal stability curve (figure 6*a*, $\epsilon = 0.4$).

3.3.2. *Double-layer attraction*

In this subsection we examine the case in which the diffuse layers next to the fluid interface and the wall have volume charge densities ρ_e^0 of opposite sign. It is clear from (3.17) that in order to obtain diffuse layers of opposite charge the sign of Φ_1 must be opposite to Φ_w, or $\Delta\Phi/\Phi_1 > 1$. Plots of potential distributions $(\Phi - \Phi_1)/\Phi_1$ for various negative and positive values of $\Delta\Phi/\Phi_1$ appear in figure 8(*c*), and figures

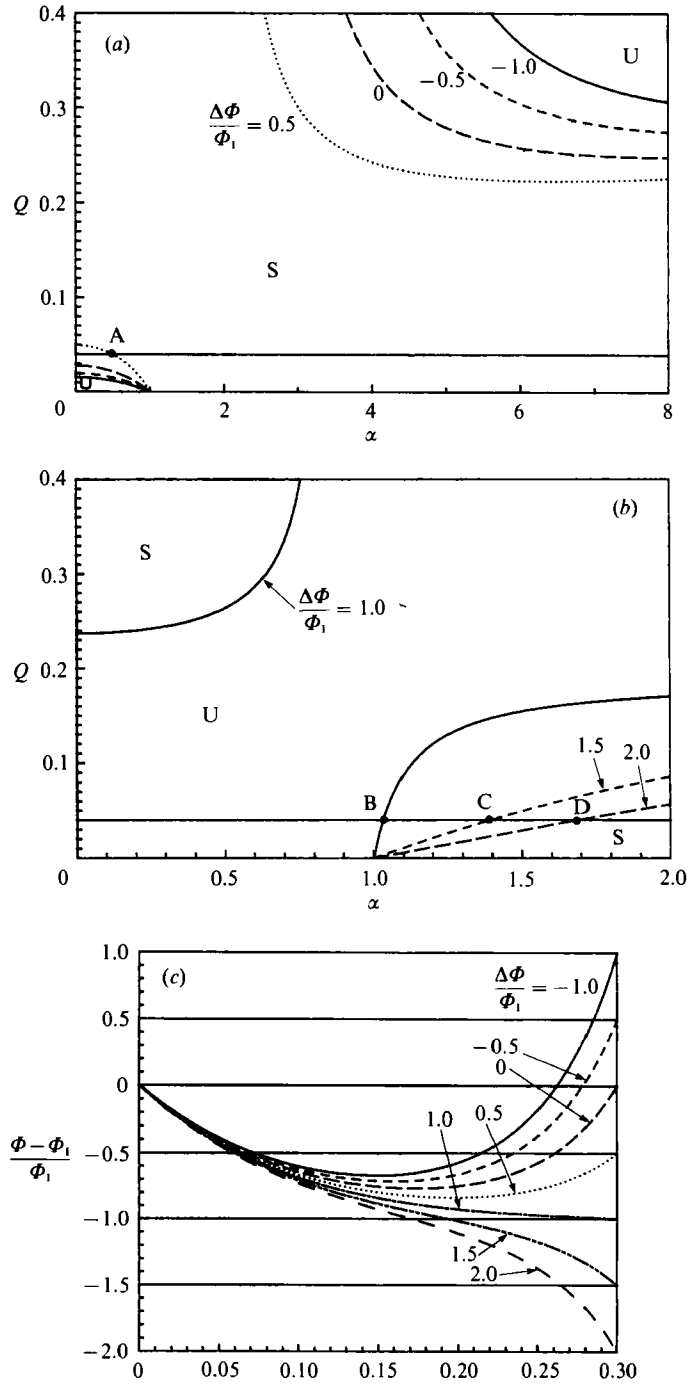

FIGURE 8. Stability of an electrolyte film in the presence of double-layer attraction due to *volume* charge density. $\epsilon = 0.3$. (*a*) Type A neutral curves of double-layer repulsion for $(\Delta\Phi/\Phi_1) < 1$, $\kappa = 10$. (*b*) Type B neutral curves resulting from double-layer attraction $[\Delta\Phi/\Phi_1] \geqslant 1$, $\kappa = 10$. (*c*) Base state electrostatic potential profiles for incrementally larger values of $\Delta\Phi/\Phi_1$; $\kappa = 10$.

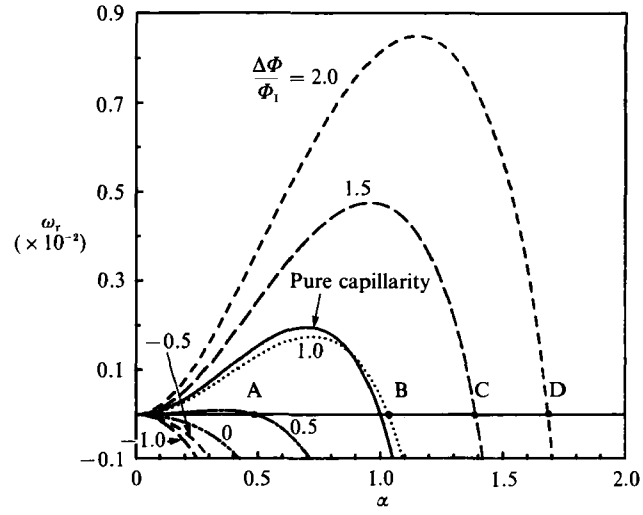

FIGURE 9. The acceleration of the growth rate in the presence of increasing double-layer attraction at fixed Q. $J = 1000$, $m = 1$, $Q = 0.04$, $\epsilon = 0.3$, $\kappa = 10$.

8(a) and 8(b) give the corresponding neutral curves. As expected, when $\Delta\Phi/\Phi_1 \leqslant 1$ and the volume charge density is everywhere of the same sign, the double layers repel, and for the values of ϵ and κ chosen (0.3 and 10, respectively) in figure 8(a), type A neutral curves characterizing strong double-layer repulsion obtain. As $\Delta\Phi/\Phi_1$ increases from 1, the charge of the diffuse layers next to the wall and next to the fluid interface take on opposite signs. This change in diffuse layer sign destabilizes the system because in regions where the film thickness has decreased charges of unlike sign (favourably) approach one another.

As $\Delta\Phi/\Phi_1$ increases from an initially strong double-layer repulsion configuration, b_0 decreases and b_2 increases, and the unstable lobe of the type A neutral curves grows. At a critical value of $\Delta\Phi/\Phi_1$ (≈ 1 for the values of ϵ and κ chosen) b_2 becomes greater than b_0, and a transition back to type B neutral curves occurs (figure 8b). Finally, as $\Delta\Phi/\Phi_1$ increases further, b_0 decreases through zero to negative values and the upper branch of the type B curves disappears leaving only the lower branch. This branch (described by (3.15) when $Qb_2 < 1$) recedes with increasing $\Delta\Phi/\Phi_1$ as b_2 increases, i.e. the stabilization of the axial curvature decreases. Finally, as in the previous cases the lower branch of figure 8(b) goes as $O(\alpha)$ for $\alpha \to \infty$; thus in the case of double-later attraction for which there is only one branch ($b_0 \leqslant 0$), the system becomes unstable to an increasingly wider band of wavelengths as Q increases.

Figure 9 shows the influence of double-layer attraction on the growth rate for $m = 1$, $J = 10^3$ and $Q = 0.04$ and for the same values of ϵ and κ as in figure 8. Points A, B, C and D in figures 8(a), 8(b) and 9 are the wavelengths of zero growth. Figure 9 shows that as double-layer repulsion fades (increasing $\Delta\Phi/\Phi_1$) the window of stability disappears and as double-layer attraction takes over, the maximum growth rate and the wavenumber of maximum instability increase until they exceed those for pure capillarity.

Double-layer attraction can also occur even when the volume charge density is everywhere of the same sign if the *surface* charge densities of the two interfaces (film–core and film–tube) are of opposite sign. This can be achieved either by reducing the film thickness ϵ keeping the Debye length ($1/\kappa$) constant or by increasing the Debye length (decreasing κ) keeping the film thickness constant, in the

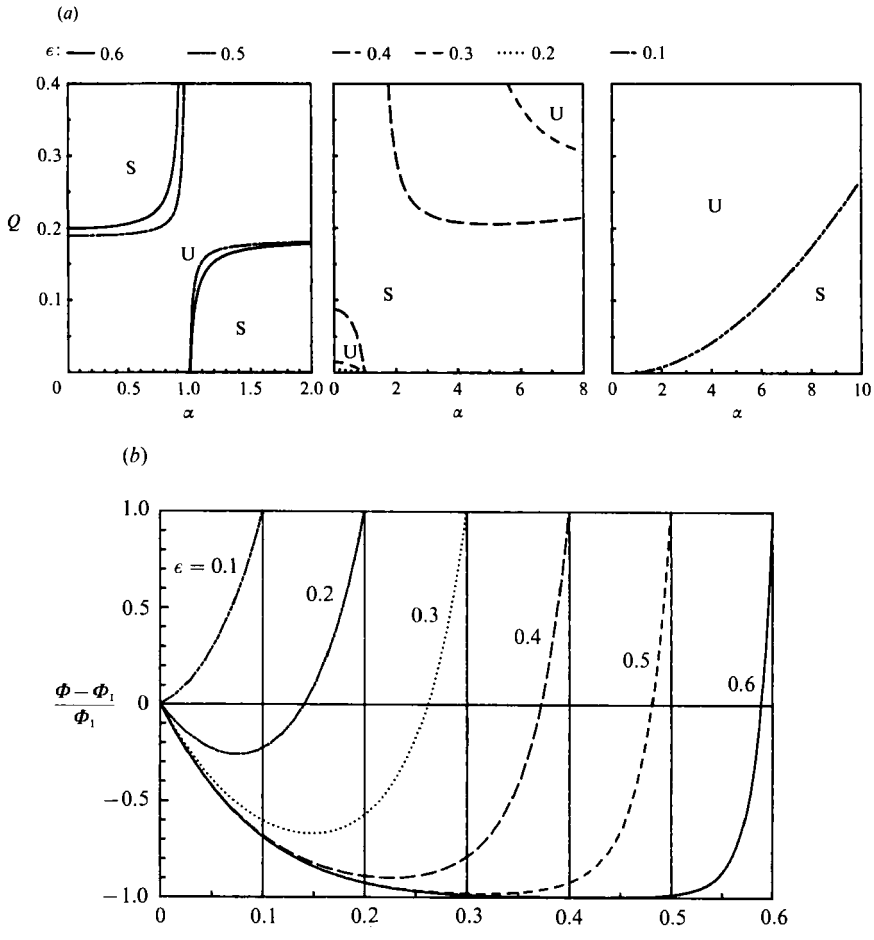

FIGURE 10. Stability of an electrolyte film in the presence of double-layer attraction due to *surface* charge density. $\kappa = 10$, $\Delta\Phi/\Phi_I = -1$. (*a*) The ϵ-dependence of neutral curves for $\Delta\Phi/\Phi_I \neq 0$. (*b*) Base state electrostatic potential profiles for different values of ϵ and $\Delta\Phi/\Phi_I \neq 0$.

case where the potential difference $\Delta\Phi$ is fixed and non-zero. This can be shown as follows. First the governing equation (2.21) for the base state potential is

$$\frac{d^2\Phi^0}{dr^2} + \frac{1}{r}\frac{d\Phi^0}{dr} = \kappa^2\Phi^0; \tag{3.21}$$

then by defining a film variable y as $\epsilon y = 1/(1-\epsilon) - r$, and letting ϵ go to zero ($\epsilon \to 0$) one gets

$$\frac{d^2\Phi^0}{dr^2} = 0. \tag{3.22}$$

The solution of (3.22) is linear with respect to r, so when $\Delta\Phi \neq 0$ the surface charge densities ($\sigma_e = -\boldsymbol{n}\cdot\nabla\Phi^0$) of the two interfaces are of opposite sign. On the other hand if one lets the Debye length go to infinity ($\kappa \to 0$), then (2.21) becomes

$$\frac{d^2\Phi^0}{dr^2} + \frac{1}{r}\frac{d\Phi^0}{dr} = 0. \tag{2.23}$$

The solution of (2.23) is $\Phi^0 = d_1 \ln(r) + d_2$ which does not have an extreme; so, again the surface charge densities of the interfaces are of opposite sign.

Figure 10(*b*) shows plots of potential distributions $(\Phi - \Phi_I)/\Phi_I$ for some decreasing values of the film thickness ($\epsilon = 0.6, 0.5, 0.4, 0.3, 0.2, 0.1$). It is clear from that figure that as the film thickness decreases the potential distribution in the film becomes linear and the surface charge density at the film–core interface changes sign. Figure 10(*a*) shows the corresponding neutral curves. As expected, when the two interfaces are far apart ($\epsilon = 0.6$ and 0.5) we get type B neutral curves, similar to the ones from the infinite outer region case. When the interfaces are brought closer together ($\epsilon =$ 0.4, 0.3 and 0.2) the double layers repel and type A neutral curves characterizing double-layer repulsion obtain. At some critical film thickness, which is a function of the Debye length and the potential difference, the potential distribution becomes linear, forcing the surface charge densities of the two interfaces to become of opposite sign; a strong double-layer attraction results (see right-hand graph in figure 10*a*). Similar neutral curves arise for the second case ($\kappa \to 0$).

4. Summary and conclusions

The results presented in §3 bear directly on the critical question of how to stabilize an annular film from the capillary instability. Figures 6(*a*) and 8(*a*) have windows of Q-values that emerge only when the volume charge density is everywhere of the same sign. In such cases double-layer repulsion is strong enough to stabilize the action of the circumferential curvature while not at the same time reducing the surface energy to the point where the axial curvature tension is no longer positive (i.e. $1/b_0 < Q < 1/b_2$). For moderate ϵ and κ, decreasing $\Delta\Phi/\Phi_I$ may realize this. Physically, decreasing $\Delta\Phi/\Phi_I$ proceeds when one sets the wall potential higher than that of the reservoir for $\Phi_I > 0$. Then, at fixed ϵ and κ, a decrease in $\Delta\Phi/\Phi_I$ brings on and then widens a band of complete stability (cf. figures 8*a* and 8*b*). Alternatively, for fixed, negative Φ_w, adsorption of an anionic surfactant can force Φ_I negative by lowering the interface potential relative to the bulk.

Consider, as a numerical example of complete stabilization, an electrolyte film surrounding an oil core in a rock pore with a characteristic diameter of 100 μm and with the anionic surfactant sodium dodecal sulphate (SDS) introduced in the electrolyte film. SDS adsorbs onto the oil–water interface creating a surface potential. In this numerical example, we assume that the surfactant also adsorbs onto the rock wall in the same way that it adsorbs to the oil–water interface so that the potential difference between the two interfaces is zero ($\Delta\Phi = 0$). Havenbergh & Joos (1983) and Bleys & Joos (1985) have shown that the adsorption of SDS at the air–water interface may be described by a Langmuir adsorption isotherm:

$$\sigma_e = -e\Gamma^- = -e\frac{\Gamma^-_\infty \rho_e^-(r=f)}{a + \rho_e^-(r=f)}, \tag{4.1}$$

where Γ^- is the surface surfactant concentration, Γ^-_∞ is the maximum surface surfactant concentration, a is the Langmuir constant and $\rho_e^-(r=f)$ is the volume charge density at the interface. The constants a and Γ^-_∞ have been calculated for the air–water interface. Assuming the same constants for adsorption onto an oil–water interface, one can calculate the surface charge density and surface potential. Then from (2.43) one can find the critical surface tension corresponding to the lower branch of the window of stability of type A neutral curves ($Q = 1/b_0$). Systems with surface tension below this critical value can lie in the window and be stable. Figure 11 shows

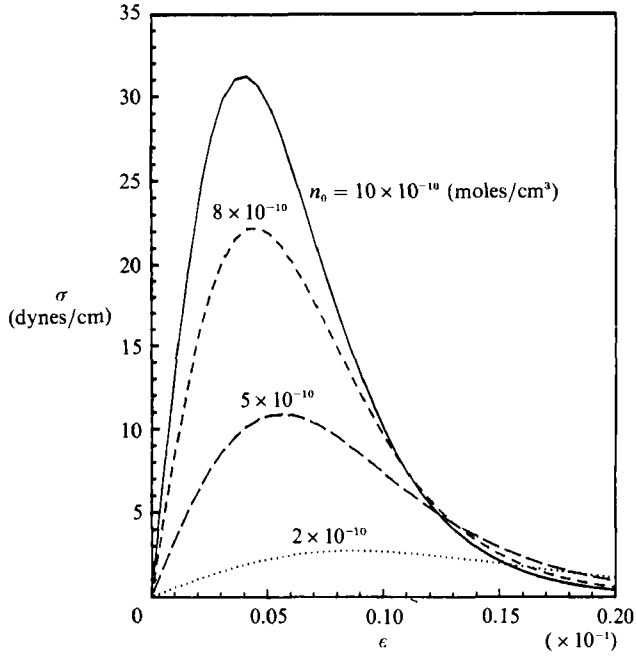

FIGURE 11. Numerical example of complete stabilization (critical surface tension versus ϵ). $R_1 = 100$ μm.

curves of the critical surface tension versus the film thickness ϵ for various values of the surfactant concentration n_0. From this figure we see that, as an example, if the oil–water interfacial tension of the system is reduced to 10 dynes/cm (by, say, introducing a second, non-ionic surfactant), then for a trace surfactant concentration of SDS $n_0 = 8 \times 10^{-10}$ mole/cm^3 the system can become stable for film thicknesses in the range ($\epsilon = 0.001$ to 0.01). When surface potentials exceeding the Debye–Hückel limit are necessary, for this regime, the above theory can only be used as a guideline for the calculation of stability windows.

This band window of stability which occurs with double-layer repulsion represents the only case of stability to all wavelengths. In an infinite system ($R_2 \to \infty$ or $\epsilon \to 1$) this stabilization is not possible: although surface tension lowering can stabilize the circumferential tension at long waves (when $Qb_0 > 1$), $b_2 > b_0 > 0$ implies that the longitudinal tension is necessarily also negative ($Qb_2 > 1$), which leads to an unstable band for moderate wavenumbers (cf. figure 4). This behaviour, however, both in the infinite case and in the finite case for weak or non-existent double-layer repulsion can be advantageous for the emulsification of the fluids, i.e. to produce fluid droplets that have radii significantly smaller than R_1.

This work was supported in part by grants from the National Science Foundation to D.R. (Grants CBT 8505654 and CBT 8658147) and the Department of Energy to C.M. (Grant DE-FG02-88ER13820).

Appendix

The parameter b_2 from §3.3 is given by

$$b_2 = \left[\frac{\Phi_r^0}{\Phi_I}\right]^2 \left[\frac{\hat{\alpha}_1 K_1(\kappa) + \hat{\alpha}_2 K_2(\kappa) + \hat{\alpha}_3 K_3(\kappa) + \hat{\alpha}_4 K_0(\kappa) K_0(\kappa a) + \hat{\beta}_0 K_0^2(\kappa a) - \hat{\beta}_2 K_2(\kappa a)}{8\kappa (I_0(\kappa) K_0(\kappa a) - I_0(\kappa a) K_0(\kappa))^2}\right] \tag{A 1}$$

where

$$\hat{\alpha}_1 = [\hat{\alpha}_{11} + (\kappa^2 - 8) I_0(\kappa) I_0(\kappa a)] K_0(\kappa a) + (\kappa^2 - 8) I_0^2(\kappa a) K_0(\kappa), \tag{A 2}$$

$$\hat{\alpha}_2 = 2\kappa^2 I_0(\kappa a) (I_0(\kappa a) K_1(\kappa) + K_0(\kappa a) I_1(\kappa)), \tag{A 3}$$

$$\hat{\alpha}_3 = \kappa^2 I_0(\kappa a) (I_0(\kappa) K_0(\kappa a) - K_0(\kappa) I_0(\kappa a)), \tag{A 4}$$

$$\hat{\alpha}_4 = ((8 - \kappa^2) I_1(\kappa) - I_3(\kappa)) I_0(\kappa a) + 2\kappa^2 a^2 I_1(\kappa) I_2(\kappa a), \tag{A 5}$$

$$\hat{\beta}_0 = (I_3(\kappa) + I_1(\kappa)) \kappa^2 I_0(\kappa) - (8 I_0(\kappa) + 2\kappa^2 I_2(\kappa)) I_1(\kappa), \tag{A 6}$$

$$\hat{\beta}_2 = 2a^2 \kappa^2 I_0(\kappa a) (I_0(\kappa) K_1(\kappa) + K_0(\kappa) I_1(\kappa)), \tag{A 7}$$

and

$$\hat{\alpha}_{11} = 2(a^2 I_0(\kappa) I_2(\kappa a) - I_2(\kappa) I_0(\kappa a)). \tag{A 8}$$

REFERENCES

Abramowitz, M. & Stegun, I. A. 1972 *Handbook of Mathematical Physics.* Dover.

Bleys, G. & Joos, P. 1985 Adsorption kinetics of bolaform surfactants at the air/water interface. *J. Phys. Chem.* **89**, 1027–1032.

Chandrasekhar, S. 1968 *Hydrodynamic and Hydromagnetic Stability.* Oxford University Press.

Felderhof, B. U. 1968 Dynamics of free liquid films. *J. Chem. Phys.* **49**, 44–51.

Frenkel, A. L., Babchin, A. J., Levich, B. G., Shlang, T. & Sivashinsky, G. I. 1987 Annular flows can keep unstable films from breakup: nonlinear saturation of capillary instability. *J. Colloid Interface Sci.* **115**, 225–233.

Gallez, D. & Coakly, G. 1986 Interfacial instability at cell membranes. *Prog. Biophys. Molec. Biol.* **48**, 155–199.

Goren, S. L. 1962 The instability of an annular thread of fluid. *J. Fluid Mech.* **27**, 309–319.

Havenbergh, J. V. & Joos, P. 1983 The dynamic surface tension in a free falling film. *J. Colloid Interface Sci.* **95**, 172–181.

Hickox, C. E. 1971 Instability due to viscosity and density stratification in axisymmetric pipe flow. *Phys. Fluids* **14**, 251–262.

Hu, H. H. & Joseph, D. D. 1989 Lubricated pipelines: stability of core–annular flow. Part 2. *J. Fluid Mech.* **205**, 359–396.

Jain, R. K. & Maldarelli, M. 1988 The hydrodynamic stability of thin films. In *Thin Films* (ed. I. B. Ivanov). Marcel Dekker.

Joseph, D. D., Renardy, Y. & Renardy, M. 1984 Instability of the flow of immiscible liquids with different viscosities in a pipe. *J. Fluid Mech.* **141**, 309–317.

Melcher, J. R. 1981 *Continuum Electromechanics.* MIT Press.

Melcher, J. R. & Taylor, G. I. 1969 Electrohydrodynamics. *Ann. Rev. Fluid Mech.* **1**, 111–146.

Miller, C. A. & Scriven, L. E. 1970*a* Interfacial instability due to electrical forces in double layers. (I). General considerations. *J. Colloid Interface Sci.* **33**, 360–370.

Miller, C. A. & Scriven, L. E. 1970*b* Interfacial instability due to electrical forces in double layers. (II). Stability of interfaces with diffuse layers. *J. Colloid Interface Sci.* **33**, 371–383.

Papageorgiou, D. T., Maldarelli, C. & Rumschitzki, D. S. 1990 Nonlinear interfacial stability of core–annular film flow. *Phys. Fluids* A **2**, 340–352.

Preziosi, K., Chen, K. & Joseph, D. D. 1989 Lubricated pipelines: stability of core–annular flow. *J. Fluid Mech.* **201**, 323–356.

Rayleigh, Lord 1879 On the capillary phenomena of jets. Appendix I. *Proc. R. Soc. Lond.* A **29**, 71.

RAYLEIGH, LORD 1892 On the instability of a cylinder of viscous liquid under capillary force. *Phil. Mag.* **34**, 145.

SAEZ, A. E., LARBENIELL, K. G. & LEREC, J. 1986 The hydrodynamics of trickling flow in packed beds I: Conduit models. *AIChE J.* **32**, 353.

SAVILLE, D. A. 1970 Electrohydrodynamic stability: fluid cylinders in longitudinal electric fields. *Phys. Fluids* **13**, 2987–2994.

SAVILLE, D. A. 1971 Electrohydrodynamic stability: effects of charge relaxation at the interface of a liquid jet. *J. Fluid Mech.* **48**, 815–827.

TOMOTIKA, S. 1935 On the stability of a cylindrical thread of a viscous liquid surrounded by another viscous liquid. *Proc. R. Soc. Lond.* A **150**, 322–337.

YIH, C. S. 1967 Instability due to viscosity stratification. *J. Fluid Mech.* **27**, 337–352.